RSC Advances

ROYAL SOCIETY OF CHEMISTRY

www.rsc.org/advances

RSC Advances

Cite this: DOI: 10.1039/c0xx00000x

www.rsc.org/xxxxxx

ARTICLE TYPE

Porous Micro-spherical $LiFePO_4$/CNT Nanocomposite for High Performance Li Ion Battery Cathode Material

Wei Wei[a,b], Linlin Guo[a,b], Xiaoyang Qiu[a], Peng Qu[a]*, Maotian Xu[a]* and Lin Guo[b]*

Received (in XXX, XXX) Xth XXXXXXXXX 20XX, Accepted Xth XXXXXXXXX 20XX
DOI: 10.1039/b000000x

Although many routes have been developed that can efficiently improve the electrochemical performance of $LiFePO_4$ (LFP) cathode for Li ion batteries, few of them meet the urgent industrial requirements: large scale production, low cost and excellent performance. In this work, via a hydrothermal synthetic proceed followed by a high-temperature lithiation, we are able to design porous micro-spherical LFP/Carbon Nanotubes (CNTs) nanocomposite. The efficient combination of the inside CNTs and the outside carbon layer, as well as the porous structure of the LFP/CNT nanocomposite lead to its excellent electrochemical performance. As cathode material for Li ion batteries, the discharge capacity of the nanocomposite can reach 122 mAh/g at 20 C. After 500 cycles, capacity retention of 94.3 % can be reached at 1 C. Because of the facile and easily scale up synthsized method, low cost raw materials and the excellent electrochemical performance, the as-designed LFP/CNT nanocomposite can be expected as a potential cathode candidate for Li ion batteries.

1 Introduction

By the 21st century, energy crisis becomes one of the great challenges. Development of environmentally benign, sustainable, and renewable energy is economically and environmentally critical, in response to the increasing energy needs of modern society and the emerging ecological concerns. Utilizing renewable energy sources, such as solar power, wind and ocean waves, is an important step toward the worldwide imperative to replace the inevitably vanishing non-renewable fossil fuel and avoid negative effects from the current combustion-based energy and environmental problems. With the fast development of technology, the converse of the renewable energies to electricity is no longer challenge. The new urgent challenge is the necessity of efficient electricity storage devices due to the widely use of large electrical appliances such as electric vehicles (EVs), hybrid electric vehicles (HEVs) and so on.

Li ion batteries (LIBs) have been considered as one of the most promising environmentally friendly energy conversion and storage devices because of their unique advantages including high energy density and long cycle life.[1-4] However, more efforts are still needed to upgrade the performance of LIBs for their further applications in EVs and HEVs, because they require high capacity, power density and safety. Electrode materials especially cathode materials are determining factor to the performance of the LIBs.[5-8] Among reported cathode materials, LFP, with many appealing features such as long cycle life, high capacity (170 $mAhg^{-1}$), good safety, low cost, suitable voltage (3.4 V versus Li^+/Li), environmental friendliness and high thermal stability,[5, 9-11] has been considered as a promising cathode candidate for the next generation LIBs. However, the major drawback of olivine-structured LFP is the poor intrinsic electronic and lithium ion conductivities arising from the lack of mixed valency and the one-dimensional lithium ion diffusion, which influence its high electrochemical performance, especially high rate capability.[5, 9-13]

In the past decade, it is found that the electrochemical performance of LFP can be greatly improved by coating a conductive layer,[14, 15] doping ions[16, 17] and reducing particle size.[18–20]

In fact, the biggest obstacle to the commercial application of LFP is not the poor electrochemical performance now, but lack of large-scale synthesis techniques that promise it with both excellent performance and low cost. In recent years, various synthesis routes were developed to prepare LFP, including mechanical alloying,[21, 22] sol–gel methods,[23, 24] co-precipitation,[25] microwave processes,[26] hydrothermal routes,[27, 28] emulsion drying synthesis,[29, 30] carbothermal reduction method,[31] vapor deposition,[32] spray solution technology,[33] and so on. However, most methods reported were either high cost or impractical due to complicated synthesis proceed that were difficult to expand to large-scale industrialization. Even though the solid-state reactions are universally recognized as a useful methodology to prepare LFP, the drawback associated with this method is that this approach suffers from polydispersed growth of the grains due to the high processing temperatures, which greatly decreased its electrochemical performance. Therefore, it is significant to develop economic and efficient synthesis routes for the practical application of LFP materials.

In the present work, we modified our previously published result,[34] and are able to synthesis porous micro-spherical LFP/CNT nanocomposite by employing a facile hydrothermal method followed a lithiation process. When tested as cathode material for Li ion batteries, the LFP/CNT nanocomposite electrode shows a high discharge capacity of 122 mAh/g at the current rate of 20 C, and a capacity retention of 94.3 % at 1 C

after 500 cycles.

The as-designed LFP/CNT nanocomposite has a great application potential as the urgently needed Li ion battery cathode material suitable for EVs and HEVs due to the following reasons. Firstly, the raw materials (include $Fe(NO_3)_3$, $NH_4H_2PO_4$, LiOH and small amount of CNTs) are inexpensive; Secondly, the synthetic method are easily scaled-up, because it only involves two steps, the hydrothermally fabricated $FePO_4$/CNT microspheres and the following liathiation process (Doing together with the calcinations of the products). For the hydrothermal method, it is now a common industrial method to synthesis $LiFePO_4$, and the following liathiation process basically equals the calcinations process which also involves in the hydrothermally synthesized $LiFePO_4$. Thirdly, the excellent electrochemical performance as mentioned above.

2 Experiments

Preparation of materials: Multiwall CNTs (20 ~ 30 nm in diameter and 0.5 ~ 2 μm in length, Beijing jindao Reagent) were pretreated according to the method reported elsewhere.[35, 36] In the typical synthesis of LFP/CNT nanocomposite, 0.3 g of the as-prepared CNTs was first dispersed in 400 ml purified water and stirring for 10 min. Then, 0.1 mol $Fe(NO_3)_3 \cdot 9H_2O$ (≥ 99.5%, Aladdin) was dissolved in the CNT solution with ultrasonic treatment for 10 min. Thereafter, 0.1 mol $NH_4H_2PO_4$ (≥ 99.5%, Aladdin) was introduced to the above solution under stirring. After stirring for 30 min, the mixture was transferred into a 400 ml PTFE inner steel autoclave and heated at 180 °C for 10 h. The autoclave was naturally cooled to room temperature. The obtained dark green slurry was washed with de-ionized water for several times, dried under vacuum at 80 °C and obtained $FePO_4$/CNT powder precursor.

The lithiation proceed was achieved as follows: 1 g glucose and 0.1 mol $LiOH \cdot H_2O$ was mixed with the as-prepared $FePO_4$/CNT powder. The obtained mixture powder was grounded carefully with a mortar and a pestle and then transferred to a tube furnace, where it was annealed under reducing atmosphere. The tube was purged with 10% hydrogen and 90% argon for 0.5 h before heating started (flow rate: 150 cc/min). The powders were firstly heated at the rate of 5 °C min^{-1} to 300 °C and kept for 1 h. Then, the temperature was increased to 700 °C at the same heating rate and held for 10 h. Finally, ~ 16 g of LFP/CNT nanocomposite was obtained after naturally cooled to the ambient temperature.

Characterizations: Characterization details can be found in our previously published paper.[34]

Electrochemical performance: Electrochemical reactions of samples with lithium were investigated using a simple two-electrode cell. The working electrode consists of 90 wt.% LFP/CNT nanocomposite active material, 5% carbon black as conductive agent, 5 wt.% polyvinylidene fluoride (PVDF) as binder, and Al foils as substrate (current collector). N-methyl pyrrolidinone (NMP) slurry consisting of the above mixture was uniformly coated on an aluminum disk of 14 mm in diameter. The disk electrodes were dried overnight at 60 °C under vacuum followed by compression at 1.0×10^6 Pa. The 2016 type coin cells were assembled in an Ar-filled glove box using polypropylene (PP) micro-porous film as the separator, a solution of 1 M $LiPF_6$ in ethylene carbonate (EC)/dimethyl carbonate (DMC) (1:1, v/v) as electrolyte and metallic lithium foil as counter electrode. The electrochemical tests were performed on Land CT2001A battery testing systems (Jinnuo Electronics Co. Ltd., China). The charging and discharging tests were performed galvanostatically at various currents and at a constant temperature of 25 °C in the voltage ranging from 2.0 to 4.2 V. The electronic conductivity was measured at room temperature by the 4-probe method. The LFP/CNT powder was dried at 120 °C in vacuum for 10 h and pressed into pellets under 10 MPa at room temperature. Electrical measurements were performed with Keithley 2400 Digital Source Meter.

3 Results and Discussion

The synthetic process of LFP/CNT nanocomposite is schematically illustrated in Scheme 1. As mentioned in the experimental section, the CNTs were pretreated before used. The pretreatment is known to create oxygen-containing surface functional groups on the chemically inert surface of CNTs, thus facilitating the absorption of Fe^{3+} cations.[37] When $Fe(NO_3)_3$ solution was mixed with CNTs, Fe^{3+} would be selectively bonded with the oxygenated groups by electrostatic force. After that, $NH_4H_2PO_4$ was introduced into the solution. During the subsequent hydrothermal reaction, $FePO_4$ nanocrystals were formed and assembled into microspheres with CNTs simultaneously embedded, the driving force is the reducing of the surface tension of the highly dispersed $FePO_4$ nanoparticles.[34] After a high temperature lithiation process, $FePO_4$/CNT precursor was transformed to LFP/CNT nanocomposite.

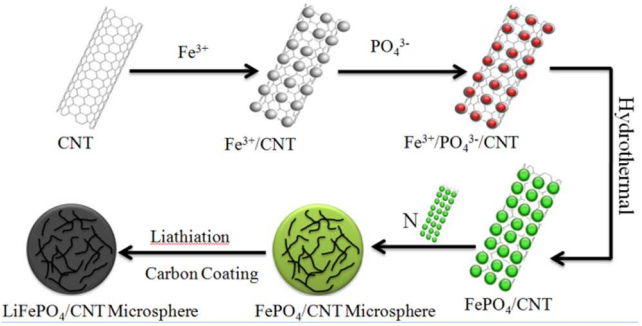

Scheme 1. Schematic illustration of the synthetic procedure for LFP/CNT.

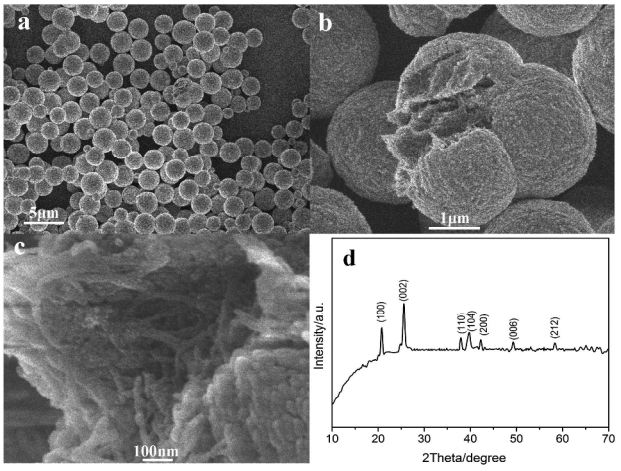

Figure 1. SEM images (a-c) of $FePO_4$/CNT nanocomposite at different magnification and (d) XRD patterns of $FePO_4$/CNT.

Fig. 1a shows the SEM image of $FePO_4$/CNTs, from which it can be found that the as-prepared product is formed in spherical morphology. Most of the mono-dispersed spheres have a particle size of ~ 3 μm in diameter, only a few spheres at 1 ~ 2μm. The SEM results indicate that even in a 400 mL autoclve, the $FePO_4$/CNT nanocomposite product can still remain their uniform micro-spherical morphology. The SEM results indicate that even

in a large scale production, the $FePO_4$/CNT nanocomposite product can still remain their uniform micro-spherical morphology, with no morphology difference compared with those prepared in small amount. [34] No obvious CNTs attach on the surface of $FePO_4$ microspheres or partially exposed, suggesting that they may be embedded in the $FePO_4$ microspheres due to their short length (0.5 ~ 2 μm). Fig. 1b shows several unbroken and broken $FePO_4$/CNT microspheres, from which it can be observed that the surface of the microspheres is smooth, no obvious mesopores exist. Fig. 1c is the magnification part of the broken $FePO_4$/CNT microspheres, we can clearly see that CNTs with a diameter of 20 ~ 30 nm are wrapped in the $FePO_4$ microspheres. Fig. 1d shows the XRD patterns of $FePO_4$/CNT, from which it can be seen well crystallized $FePO_4$ with highly purity were synthesized (matches with JCPDS card No. 29-715). No CNT related peaks can be seen, because: 1) the low content of CNTs in the composite (1.9 % in theory); 2) the CNTs may completely be embedded in the $FePO_4$ microspheres.

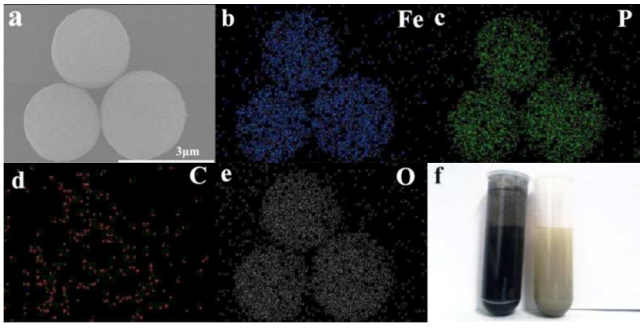

Figure 2. (a) SEM image of $FePO_4$/CNT microspheres, and (b - e) their corresponding EDS maps of Fe, P, C, O elements, (f) $FePO_4$/CNT microsphere solution before and after hydrothermal reaction.

EDS elemental mappings of $FePO_4$/CNT microspheres were performed in order to further confirm the CNTs were successfully embedded in the $FePO_4$ microspheres. Fig. 2a is the typical SEM image of three $FePO_4$/CNT microspheres, Fig. 2b-e are their corresponding Fe, P, C and O element EDS mappings, respectively. The uniform distribution of C, Fe, O and P confirms the existence and homogeneous distribution of CNTs in the $FePO_4$ microspheres. Furthermore, we compared the $FePO_4$/CNT microsphere solution before and after hydrothermal reaction. We can clearly see that, before reaction, the appearance of the solution is black, which is caused by the existence of CNTs. In contrast, the after reaction solution appears as dark green, which is consistent with the color of pure $FePO_4$. The dramatic changes in color of the solution before and after hydrothermal reaction indicating that the CNTs were successfully embedded in the $FePO_4$ microspheres. Due to the excellent electronic conductivity of CNTs, a three dimensional (3D) conductive network of the $FePO_4$ microsphere is constructed.

After the high-temperature chemical lithiation process, we obtained carbon coated LFP/CNT nanocomposite. Fig. 3a shows the TEM image of an individual LFP/CNT microsphere, from which the primary LFP nanocrystals size can be estimated at the range of 50 ~ 200 nm. High-resolution transmission electron microscopy (HRTEM) was performed to reveal the detailed microstructure of the carbon coated surface of LFP/CNT microsphere. From Fig. 3b we can clearly see that a carbon layer at around 3.5 nm in thickness is presented on the surfaces of the primary LFP nanocrystals, indicating at the high temperature liathiation process, the decomposed carbon of glucose were successfully coated on the surface of the LFP microspheres. The carbon layer can further enhance the electronic conductivity of the LFP/CNT microspheres. The *d* spacing of 0.35 nm matches with the (111) plane of LFP.

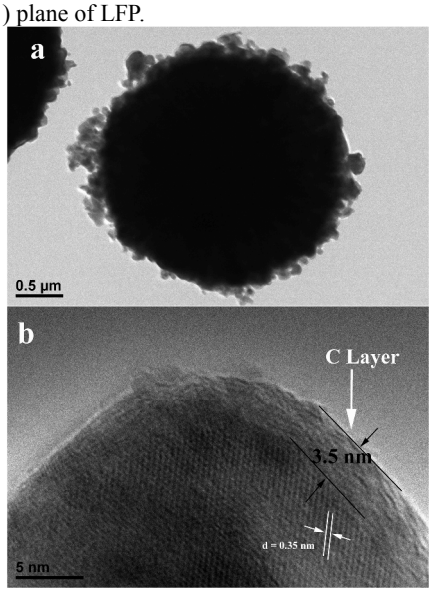

Figure 3. (a) TEM and (b) HRTEM images of an individual LFP/CNT microsphere.

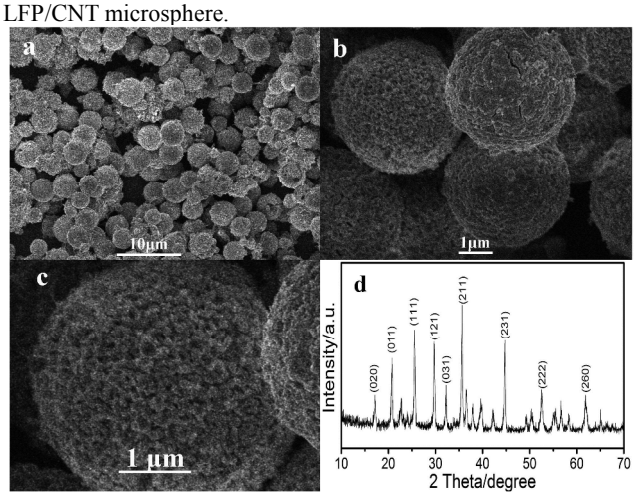

Figure 4. (a) Low and (b) high magnified SEM images of the LFP/CNT microspheres, (c) SEM image of an individual LFP/CNT microsphere and (d) XRD patterns of the LFP/CNT microspheres product.

The morphology of the LFP/CNT nanocomposite is shown in **Fig. 4** a-c. Fig. 4a is the overview of the composite, it can be seen that after the high temperature lithiation process most of the LFP/GNs still remain the spherical morphology of their precursor. The regular micro-spherical morphology promises the LFP/CNT nanocomposite with high tap density, because micro-sized spherical particles can avoid a lot of vacant space between the particles and bad fluidity of the powders while irregular particles cannot.[34] As determined by the tap density meter, the nanocomposite exhibit a high tap density up to 1.54 g/cm^3. In fact, the tap density of LFP is an important factor that has greatly influence on its final energy density. Fig. 4b is close view of several LFP/CNT microspheres,we can find that the diameter of the LFP/CNT microspheres (~ 4μm) is larger than their precursor (~ 3μm), this may caused by the following liathiation and surface carbon coating. In addition, the surface of the microspheres after liathiation process becomes rougher compared with their precursor. Fig. 4c is the close SEM depicts of an individual LFP/CNT microsphere, from which two factors are verified:

Firstly, the microspheres are consisted of LFP nanocrystals with a particle size at around 100 nm; Secondly, abundant of mesopores are existed in the surface of the microsphere. The crystal structure of the nanocomposite is investigated by using XRD techniques, as shown in Fig. 4d, all the diffraction peaks of the nanocomposite are well matched with orthorhombic phase LFP (space group *Pnma*, JCPDS Card No: 81-1173), indicating high purity LFP was formed. The average particle size determined by the peak broadening is 98.3 nm (By using the major diffraction peak (011), (111) and (211), then take the average value), in agreement with the TEM and SEM analysis.

The typical hysteresis in nitrogen adsorption/desorption isotherms in Fig. 5 reveals the porous characteristic of this intriguing LFP/CNT nanocomposite with abundant mesopores. The BET surface area is arrived at 58.46 m^2/g, the high surface area is probably derived from the mesoporous structure and high-dispersed $LiFePO_4$ microspheres (Fig. 4). The sufficient porosity in the microsphere maybe attributed to the high temperature liathiation process and the evaporation of hydrate water in the $FePO_4$ microspheres. The Barrett-Joyner-Halenda (BJH) pore-size distribution, shown in the inset of Fig. 5, indicates the LFP/CNT have an average pore diameter of 10 ~ 50 nm. The significant porosity in cathode materials can facilitate the access and accommodation of electrolyte and shorten the diffusion length of lithium ions to achieve high power density in electrode materials. [34]

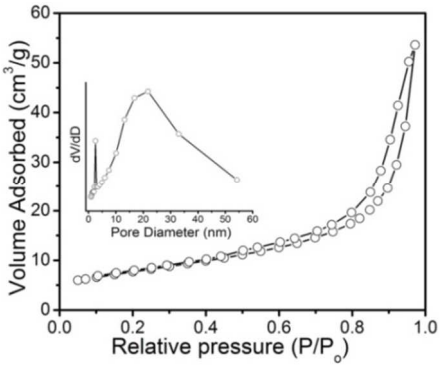

Figure 5. Nitrogen adsorption/desorption isotherms of the LFP/GNs. Inset: the pore size distribution plot calculated by the BJH formula in the desorption branch isotherm.

Thermogravimetric (TG) measurement was used to estimate the carbon content (CNTs and the glucose decomposed carbon) in the LFP/CNT sample. Fig. 6 gives the TG curves of LFP/CNT nanocomposite tested in oxygen. It should be mentioned that, in the temperature range of 250 ~ 500 °C, olive LFP is oxided to $Li_3Fe_2(PO_4)_3$ and Fe_2O_3, corresponding to a theoretical weight gain of 5.07%.[11,34] For the LFP/CNT, at 750 °C, the oxidation of both LFP and carbon is completed and the weight of the sample keeps constant. Thus, by taking into account the weight gain of pure LFP (5.07 %) and the actual weight gain of the LFP/C composite (2.31 %) during TG measurement, the total mass ratio of 2.63 % of carbon in the composite can be calculated as following:[34]

$$C_{weight}\% = 1 - (1 + 2.31\%) / (1 + 5.07\%) = 2.63\%$$

In general, the optimal carbon content in LFP/C is less than 5 wt.%,[38] this is because too much carbon would greatly reduce the final tap density of LFP due to the low density of carbon, while insufficient carbon could not guarantee the good conductivity of the material. This means the 2.63 wt.% carbon would contribute to the high tap density of the LFP/CNT nanocomposite. The total carbon loading 2.63 % include CNT and amorphous carbon, due to the nearly 100 % yiled of the $LiFePO_4$ product, the CNT and amorphous carbon loading can be generally calculated as 1.88% and 0.75%, respectively.

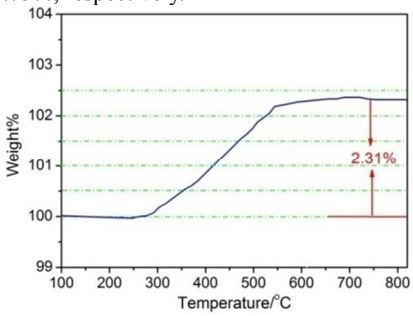

Figure 6. TGA patterns of the LFP/GNs heated in oxygen from 50 to 850 °C.

The introduction of CNTs plus the efficient carbon coating dramatically enhanced the electrical conductivity of the nanocomposite to 10.5 S cm^{-1}, which is 10 orders higher than that of pure LFP (10^{-9} S cm^{-1}).[38] The greatly improved electrical conductivity of LFP also implies the well constructed conducting network. Compared with the LFP/graphene nanocomposite we synthesized previously (the total carbon weight of the two samples are comparable, e. g. 2.63 % *vs.* 2.64 %),[34] the even higher electrical conductivity can be attributed to the following two factors: Firstly, the higher efficiency of the combination of the inside CNTs and the outside carbon layer than the single graphene layer; Secondly, the higher Li ion transport efficiency of the LFP/CNT nanocomposite than the LFP/graphene nanocomposite because Li ions cannot pass through the carbon atomic arrays in two-dimensional sheets of graphene. [39]

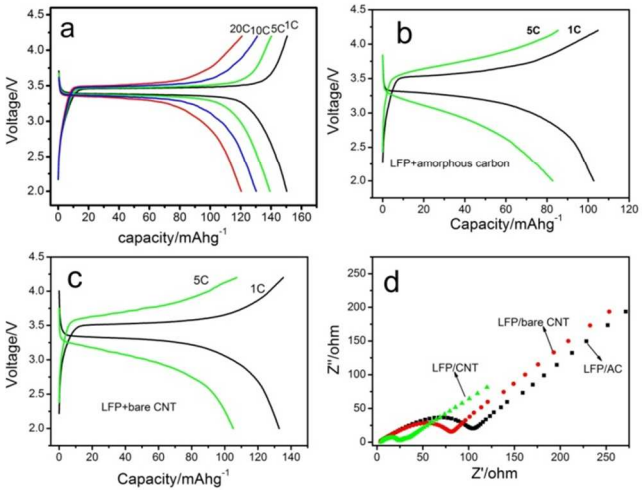

Figure 7. (a-c) charge/discharge profiles of LFP/CNT nanocomposite, LFP/AC, LFP/bare CNT at different rates, respectively; (d) the impedance spectra of the above three electrodes at 1 C rate at the end of 10 cycles.

The ionic conductivity of the as-prepared electrode was also tested by using Randles - Sevcik equation, a detail introduction can be seen in supplementary information (Fig. S1and Fig. S2, ESI†). The diffusion coefficient of Li ion obtained is 1.12×10^{-10} cm^2 s^{-1}, which is 3 ~ 4 orders higher than bare $LiFePO_4$ electrode (10^{-13} ~ 10^{-14} cm^2 s^{-1}). Therefore, the prepared ionic conductivity $LiFePO_4$/CNT electrode is greatly improved. With the both improved electronic and ionic conductivity of the electrode, we expect the excellent electrochemical performance of the $LiFePO_4$/CNT cathode.

The LFP/CNT nanocomposite electrode was cycled at different rates from 1 C to 20 C in the potential range between 2.0 and 4.2 V *vs.* Li^+/Li. At 1 C, the discharge curve is characterized

by a plateau at ~ 3.4 V, which corresponds to the reaction $LiFePO_4 \rightarrow Li^+ + FePO_4 + e^-$. The electrode capacity is 152 mAh/g, which is 89.4 % of the theoretical capacity. At higher current rates, the capacity decreases but remains as high as 140 mA h/g at 5 C, 131 mA h/g at 10 C, and 122 mA h/g at the high current of 20 C (Figure 7). In fact, the value 120 mAh/g at 20 C is not very outstanding compared with previously reported results[12, 40, 41]. What we want to emphasis is the carbon loading in the electrode, it is widely known that the higher carbon loading, the batter rate performance (for the $LiFePO_4$ electrode), however, the lower volumetric energy density. For our electrode, it is really surprising that the LFP/CNT nanocomposite can exhibiting such a good high rate capability with such a low carbon loading of 2.63% compared with the reported values[12, 40, 41]. The good high rate performance is attributed to the presence of the CNTs that efficiently connects the inside nanocrystals of the LFP microspheres and to the effective carbon layer that coated on the surface of the microspheres, both of which dramatically enhanced the electrical conductivity of the LFP/CNT nanocomposite. We performed further experiments to further confirm this conclusion, LFP/amorphous carbon (LFP/AC) electrode (prepared with the absence of CNT) and LFP/bare CNT electrode (prepared with the absence of carbon coating process) with the same carbon loading as our LFP/CNT electrode were prepared in order to make comparison. As shown in Fig. 7 b and c, at the low current rate of 1 C, the LFP/AC electrode displayed a charge/discharge capacity of 108.1 and 104.9 mAh/g, while the LFP/bare CNT electrode of 135.1 and 133.2 mAh/g; at the higher current rate of 5 C, the LFP/AC electrode shows a charge/discharge capacity of 90.1 and 84.3 mAh/g, while the LFP/bare CNT electrode of 111.3 and 106.2 mAh/g. The two electrodes exhibit much worse electrochemical performance compared with the LFP/CNT electrode. More details cyclability and rate capability data of LFP/amorphous carbon can be found in our previously published work.[34] We also performed an electrochemical impedance test with LFP/AC and LFP/bare CNT electrodes for comparison at the end of 10 cycles at 1 C rate. As can be seen from Fig. 7d, according to the Nyquist plots of the three electrodes, the LFP/CNT electrode has a charge-transfer resistance value of 24 Ω, which is smaller than that of LFP/AC (82Ω) and LFP/bare CNT (112Ω) electrode, revealing a lower charge-transfer resistance in the LFP/CNT electrode. In addition, the high surface area, the existence of abundant of mesopores plus the tubular structure of CNTs, these characteristics of the nanocomposite greatly facilitate Li ions transport across LFP nanoparticles no matter inside or outside of the microspheres. In our tests, the LFP/CNT nanocomposite was able to support current densities as high as 3400 mA/g.

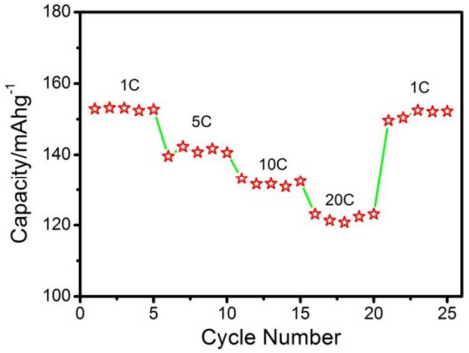

Figure 8. Rate capacities of LFP/CNT nanocomposite.

Fig. 8 shows the capacities of the LFP/CNT electrode cycled at different rates for 5 cycles at each rate. The cell capacity keeps stable, even at a rate as high as 20 C, at which the cell is fully charged or discharged within 3 min. It is worth noting that when the current density is reduced to 1 C again, the capacity returns to its original value, which indicates that, this electrode material has high recovery ability. The good recovery ability is attributed to the enwrapped-in CNTs which improve the mechanical stability of the nanocomposite and to the interconnected mesopores system that assists mass transport. Both of which endows the LFP/CNT nanocomposite the ability to withstand the stresses caused by the fast phase change from LFP to $FePO_4$, and by the infiltration of electrolyte into the nanocomposite. The result indicates that our LFP/CNT nanocomposite is tolerant to high charge/discharge currents, which is a desirable characteristic required for high power applications such as in EVs and HEVs.

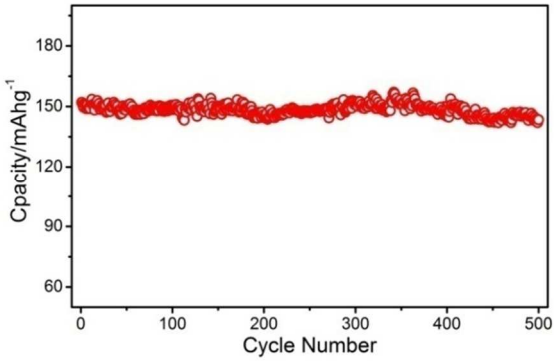

Figure 9. Cycling performance of LFP/CNT nanocomposite.

The cycling performance of the secondary batteries is extremely important to the EVs and HEVs because it directly determines their working life. Considering the practical use situation, the 1 C rate test is the most sensible. So, we carried out the long-term cycling of our LFP/CNT electrode at 1C rate. As shown in Fig. 9, the LFP/CNT electrode can deliver an initial discharge capacity of 152 mAh/g, and after 500 cycles, the capacity of 143 mAh/g can still be remained, corresponding to 94.3 % of its initial capacity. This excellent long cycling performance makes the suitable usage of our LFP/CNT nanocomposite in EVs and HEVs. The CNTs, which has good mechanical flexibility, can serves as an elastic buffer to relieve the strain during the Li ion insertion/de-insertion process which has a beneficial effect on cycling performance of the nanocomposite.

4. Conclusions

In conclusion, we have successfully designed LFP/CNT cathode for Li ion batteries. The as-prepared composite material exhibits excellent electrochemical performance: the LFP/CNT electrode can deliver a discharge capacity as high as 122 mAh/g at high current rate of 20 C; the capacity can recovery to its original value even from 20 C to 1 C; after 500 cycles the capacity retention can reach up to 94.3%. The efficient combination of the inside CNTs and the outside carbon layer as well as the porous structure, which dramatically enhanced the electronic and ionic conductivity, contribute to excellent electrochemical performance of the LFP/CNT nanocomposite. With the simple procedure and low cost materials being used, this high electrochemical performance nanocomposite has a great potential for industrial applications

Acknowledgement

This work was financially supported by the National Natural Science Foundation of China (11079002, 21475085, 21271125/B010601), and the Innovation Scientists and

Technicians Troop Construction Projects of Henan Province, Program for Innovative Research Team in Science and Technology in University of Henan Province (2012TRTSTHN018).

Notes and references

[a]*School of Chemistry and Chemical Engineering, Shangqiu Normal University, Wenhua road No. 298, Shangqiu, 476000, P. R. China.*
E-mail: qupeng0212@163.com, xumaotian@163.com
[b]*School of Chemistry and Environment, Beihang University, Beijing 100191, China.*
E-mail: guolin@buaa.edu.cn

†Electronic supplementary information (ESI) available: the calculation of the ionic conductivity of the LiFePO4/CNT electrode. See Doi:10.1039/xxxxxxxx.

1 K. S. Kang, Y. S Meng, J. Bréger, C. P. Grey, G. Ceder, *Science* **2006**, 311, 977.
2 C. K. Chan, H. L. Peng, G. Liu, K. Mcllwrath, X. F. Zhang, R. A. Huggins, Y. Cui, *Nature Nanotechnology* **2008**, 3, 31.
3 V. Etacheri, R. Marom, R. Elazari, G. Salitra, D. Aurbach, *Energy Environ. Sci. 2011*, 4, 3243-3262.
4 J. F. Liang, W. Wei, D. Zhong, Q. Yang, L. Li, and L. Guo, *ACS Appl. Mater. Interf.* **2012**, 4, 454.
5 M.S. Whittingham, *Chem. Rev.* 2004, 104, 4271.
6 F. Cheng, J. Liang, Z. Tao, and J. Chen, *Adv. Mater.* 2011, 23, 1695.
7 W. Wei, Z. Wang, Z. Liu, Y. Liu, L. He, D. Chen, A. Umar, L. Guo, J. Li, *J. Power Sources*. **2013**, 238, 376.
8. D. Chen, W. Wei, R. Wang, X. Lang, Y. Tian, and L. Guo, *Dalton Trans.* 2012, 41, 8822.
9 A. K. Padhi, K. S. Nanjundaswamy, and J. B. Googenough, *J. Electrochem. Soc.* **1997**, 144, 1188.
10 Y. K. Zhou, J. Wang, Y. Y. Hu, R. O'Hayre, and Z. P. Shao, *Chem. Commun.* **2010**, 46, 7151.
11 W. Wei, D. Chen, R. Wang and L. Guo, *Nanotechnology* **2012**, 23, 475401.
12 G. Wang, H. Liu, J. Liu, S. Qiao, G. M. Lu, P. Munroe, and H. Ahn, *Adv. Mater.* **2010**, 22, 4944.
13 X. L. Wu, L. Y. Jiang, F. F. Cao, Y. G. Guo, and L. J. Wan, *Adv. Mater.* **2009**, 21, 2710.
14 N. Ravet, Y. Chouinard, J. F. Magnan, S. Besner, M. Gauthier and M. Armand. *J. Power Sources* **2001**, 97/98, 503.
15 Y. H. Huang and J. B. Goodenough. *Chem. Mater.* **2008**, 20, 7237.
16 S. Y. Chung, J. T. Bloking and Y. M. Chiang. *Nature Mater.* **2002**, 1, 123
17 P. G. Bruce, B. Scrosati and J. M. Tarascon. *Angew. Chem. Int. Ed.* **2008**, 47, 2930
18 Y. J. Lee, H. Yi, W. Kim, K. Kang, D. S. Yun, M. S. Strano, G. Cender and A. M. Belcher. *Science* **2009**, 324, 1051
19 M. H. Lee, J. Y. Kim and H. K. Song. *Chem. Commun.* **2010**, 46, 6795
20 H. K. Song, K. T. Lee, M. G. Kim, L. F. Nazar and J. Cho. *Adv. Funct. Mater.* **2010**, 20, 3818.
21 S. Franger, F. L. Cras, C. Bourbon, H. Rounault, *Electrochem. Solid-State Lett.* **2002**, 5, A231.
22 C. W. Kim, M. H. Lee, W. T. Jeong, K. S. Lee, *J. Power Sources* **2005**, 146, 534.
23 J. Yang, J. J. Xu, *Electrochem. Solid-State Lett.* **2004**, 7, A515.
24 G. X. Wang, S. Bewlay, S. A. Needham, H. K. Liu, R. S. Liu, V. A. Drozd, J.-F. Lee, J. M. Chen, *J. Electrochem. Soc.* **2006**, 153, A25.
25 K. S. Park, K. T. Kang, S. B. Lee, G. Y. Kim, Y. J. Park, H. G. Kim, *Mater. Res. Bull.* **2004**, 39, 1803.
26 K. S. Park, J. T. Sun, H. T. Chung, S. J. Kim, C. H. Lee, H. G. Kim, *Electrochem. Commun.* **2003**, 5, 839.
27 S. Yang, P. Y. Zavalij, M. S. Whittingham, *Electrochem. Commun.* **2001**, 3, 505.
28 K. Shiraishi, K. Dokko, K. Kanamura, *J. Power Sources* **2005**, 146, 555.
29 S. T. Myung, S. Komaba, N. Hirosaki, H. Yashiro, N. Kumagai, *Electrochim. Acta* **2004**, 49, 4213.
30 T. H. Cho, H. T. Chung, *J. Power Sources* **2004**, 133, 272.
31 J. Barker, M. Y. Saidi, J. L. Swoyer, *J. Electrochem. Soc.* **2003**, 6, A53.
32 I. Belharouak, C. Johnson, K. Amine, *Electrochem. Commun.* **2005**, 7, 983.
33 K. Konstantinov, S. Bewlay, G. X. Wang, M. Lindsay, J. Z. Wang, *Electrochim. Acta.* **2004**, 50, 421.
34 W. Wei, S. Gao, Z. Yang and L. Guo, *RSC Adv.,* **2014**, 4, 56701.
35 H. Fang, S. Zhang, X. Wu, W. Liu, B. Wen, Z. Du, T. Jiang, *J. Power Sources* **2013**, 235, 95.
36 H. Fang, S. Zhang, T. Jiang, R. Lin, Y. Lin, *Electrochim. Acta* **2014**, 125, 427.
37 J. Lu, *Carbon* **2007**, 45, 1599.
38 L. X. Yuan, Z. H. Wang, W. X. Zhang, X. L. Hu, J. T. Chen, Y. H. Huang, and J. B. Goodenough, *Energy Environ. Sci.*, **2011**, 4, 269.
39 G. Kucinskis, G. Bajars and J. Kleperis, J. Power Sources, **2013**, 240, 66.